IEEE Access
Multidisciplinary | Rapid Review | Open Access Journal

Received October 10, 2020, accepted October 23, 2020, date of publication October 28, 2020,
date of current version December 17, 2020.

Digital Object Identifier 10.1109/ACCESS.2020.3034458

Emission Spectrum Analysis of Two Typical Partial Discharge Forms Under High Frequency Square Wave Voltages

YIKUN ZHAO[1,2], YANFEI LI[1,2], KANG LI[1], (Member, IEEE), DONG HAN[1,2], ZONGJIA QIU[1], AND GUOQIANG ZHANG[1,2]

[1]Institute of Electrical Engineering, Chinese Academy of Sciences, Beijing 100190, China
[2]University of Chinese Academy of Sciences, Beijing 100039, China

Corresponding author: Guoqiang Zhang (zhanggqi@mail.iee.ac.cn)

This work was supported in part by the Scientific Instrument Development Project of Chinese Academy of Sciences under Grant YJKYYQ20200012, and in part by the National Key Research and Development Program of China under Grant 2017YFB0903902.

ABSTRACT Although the increase in frequency improves the transmission efficiency of high-frequency transformer, a higher probability of insulation failure is caused by high-frequency partial discharges. Through a high-frequency experimental platform, emission spectrum tests on two types of insulation faults were carried out under high-frequency square wave voltages. Subsequently, the influence of frequency and voltage amplitude on the light intensity and the number of photons of emission spectrum caused by air corona were studied. Finally, the variation of the spectrum of the partial discharge occurring at the interface of gas-solid insulation with frequency was analyzed. The results show that, the characteristic spectrum of air corona is composed of the near-ultraviolet spectrum, which is caused by the energy level transition of N_2 molecules, and the number of photons of air corona is positively correlated with voltage amplitude and frequency. Partial discharges at the gas-solid insulation interface have band spectrums in the visible light region and the near-infrared light region except for the near-ultraviolet spectrum due to the energy level transitions of outer layer electronics and the vibrations of C-H chemical bonds of PET molecules. This paper preliminarily verified the feasibility of applying the emission spectrum diagnostic method to two typical partial faults under high-frequency square wave voltages.

INDEX TERMS High-frequency insulation, partial discharge, emission spectrum analysis.

I. INTRODUCTION

The solid-state transformer (SST) has been widely used in smart grid and distributed energy systems for its lower volume and higher transmission efficiency. SST can realize reliable integration of large-scale renewable energy and flexible connection of AC and DC power systems [1]–[3]. As the key component of SST, high-voltage high-frequency (HV-HF) transformer plays an important role in electrical isolation and power transmission [4], [5]. Since the HV-HF transformer is an intermediate module connecting the primary and secondary power electronic conversion circuits in SST. After the inverter and rectification transformation, the port voltage of HV-HF transformer is usually a non-sinusoidal signal with short risetime, large amplitude and high frequency, which approximates the square waveform, which is far from the operating conditions of power frequency transformers [6], [7]. Partial discharge (PD) caused by coupled electro-thermal stresses is the main reason for the insulation aging and premature failure under high frequency voltages. Some studies have indicated that the partial discharge properties including the number of discharges, discharge energy and phenomena under high frequency square wave voltages are different from those under the power frequency sinusoidal voltages [8]–[10].

Partial discharges are hazards for power equipment but also the important monitoring objects for insulation status diagnosis. There are three forms of partial discharge in the transformer, including air corona, partial discharge inside dielectrics and surface discharge at the gas-solid insulation interface, which will accelerate insulation degradation and eventually lead to insulation failures such as breakdown

The associate editor coordinating the review of this manuscript and approving it for publication was Qingli Li.

or flashover. Due to the partial discharge has the phenomenon of electromagnetic and acoustic wave, existing diagnostic methods for corona discharge under 50 Hz or 60 Hz mainly include the pulse current, radio frequency (RF), ultra-high frequency (UHF) and acoustic emission (AE) methods. However, HV-HF transformers are intermediate modules connecting the primary and secondary power electronic conversion circuits in SSTs [11]. Due to the existence of switching circuits, the RF, UHF and pulse current methods are subject to high-frequency electromagnetic interference, making the detection results inaccurate. The AE method is susceptible to noise from HV-HF transformer and switching circuits, which makes it unsuitable for the on-site detection. New detection methods need to be proposed for high-precision on-line monitoring of PD of HV-HF transformers.

In addition to electromagnetic radiation, acoustic waves and current flow, the light emission is another phenomenon caused by partial discharge. With the advancement of optical sensing technology, the spectral detection is gradually being used in the diagnosis of partial discharge due to its significant advantages such as being not affected by electromagnetic environment and equipment vibration, and high accuracy of detection results [12]–[14]. M. Koziol *et al* found that the emission spectrums of air corona have large differences when the shape of the electrode changes [15]. K. Fujii *et al* further performed partial discharge tests in air under four kinds of electrode shapes, and found that the emission spectrum of partial discharge in air is mainly concentrated in the wavelength range of 300∼400 nm, which belongs to the near-ultraviolet (UV) region [16]. W. Zhao *et al* proved that the light intensity in the near-ultraviolet region of air corona discharge decreases with the increasing distance between the electrodes, and increases with the increasing applied voltages [17]. M. Ren further proposed an approach for clustering analysis on the hazard types of partial discharges via spectral detection [18]. However, research on the emission spectral characteristics of PD under high-frequency non-sinusoidal voltage has not been carried out. Literature [19] studied the spectral properties of the partial discharge in N_2 in the frequency range of 20 Hz to 80 Hz, and found that the light intensity at a 337.1 nm is increased with the increasing frequency, which preliminarily showed that the frequency has an influence on the spectral properties of partial discharge.

In this paper, we tested the emission spectrum properties of two typical partial discharges that often occur in HV-HF transformers. Then, the influence of frequency and voltage amplitude on the relative light intensity and the number of photons of emission spectrum caused by air corona were studied. Finally, the variation of the emission spectrum of the partial discharge occurring at the interface of gas-solid insulation with frequency was analyzed. The analysis of the spectral properties of PDs under high frequency voltage provides a theoretical reference for the proposal of online detection of partial discharge of HV-HF transformers.

II. EXPERIMENTAL SETUP

A. PLATFORM ARRANGEMENT

Fig. 1 shows the emission spectrum test platform for partial discharges under high frequency square wave voltages. The platform is composed of five parts: a) high-frequency high-voltage power source with the output voltage range of 0∼20 kV and frequency of 1∼20 kHz, which is connected to the electrode through protective resistance; b) test chamber is used for performing PDs, and observation windows inlaid with optical glasses are opened on the outside of the chamber; c) electrical signal detection system composed of high voltage probe and oscilloscope, which is used for measuring high-frequency voltage; d) optical signal detection system composed of optical fiber probes and spectrum analyzer, which is used for detecting the wavelength and intensity of emission spectrum caused by PDs; e) Ocean View is selected as the spectral analysis software, which is used for statistics and analysis of the detected spectra. Among them, the spectrum analyzer is the MX2500+ product of Ocean Optics, with a measurable spectral wavelength range of 200 nm∼1037 nm and a resolution of 0.2 nm∼0.7 nm, and the integration time of the spectrum analyzer was set to 800 ms.

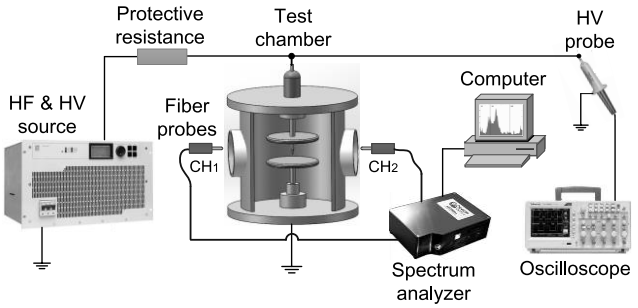

FIGURE 1. Emission spectrum test platform for partial discharge under high frequency square wave voltages.

The partial discharge test chamber is sealed to minimize background light interference, and we designed an angle-adjustable probe holder to make the fiber probe directly at the partial discharge point through the optical glass, as shown in Fig. 2(b). During the whole detection process, the edge of the electrode to be measured and the fiber probes are at the same horizontal height and the distance between them is 200 mm.

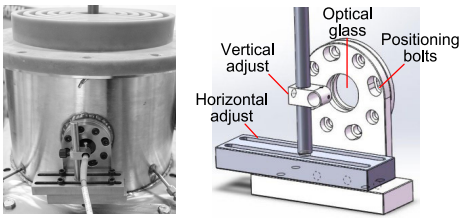

FIGURE 2. The schematic diagram of the test chamber for PDs. (a) The overall picture of test chamber. (b) Diagram of the probe holder device.

In addition, the definitions of the main signal parameters of the PDs test platform are shown in Fig. 3, and the settings

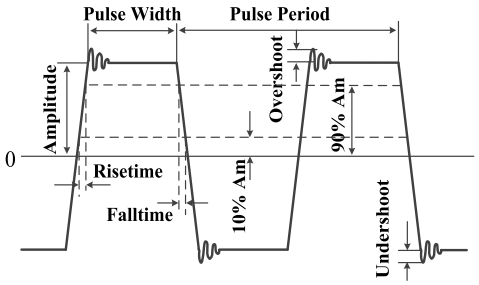

FIGURE 3. The definitions of the signal parameters of high-frequency high-voltage square wave power supply.

TABLE 1. Parameter settings of power supply.

Main Parameters	Settings
Peak-to-peak voltage	0~40 kV
Frequency	1~20 kHz
Maximum current	100 mA
Overshoot / undershoot	≤ ±5.8%
Duty cycle	50%
Rise time / fall time	8.5~10.0 μs

of signal parameters are listed in Table 1, which can fully simulate the actual port waveform of the high-voltage high-frequency transformer during the normal operation of SSTs.

B. INSULATION DEFECT MODELS OF PDs

Different kinds of insulation defects are distributed at various locations in HV-HF transformers which arise from design, manufacturing and assembling. After a period of time, the partial discharges that occur in these insulation defects will gradually evolve into breakdown or flashover accidents. In order to simulate different types of insulation defects, two defect models of partial discharge have been designed, as shown in Fig. 4. The needle-plate electrode spacing is set to 10 mm, which is used to simulate air corona in an uneven electric field. In addition, the finger electrode is used to simulate the partial discharge that occurs at the intersection of air and solid insulation materials. Two types of electrodes are made of stainless steel, and the surfaces are washed with alcohol before testing to avoid the influence of impurities.

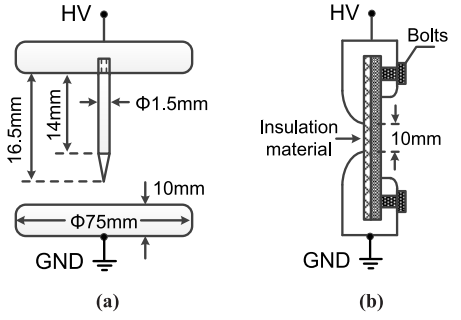

FIGURE 4. Configurations of defect models of partial discharges. (a) Needle-plate electrode. (b) Finger electrode.

The solid insulation material in partial discharge tests was selected as 6641F type of Dacron-Mylar-Dacron (DMD)

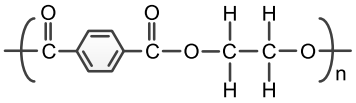

FIGURE 5. Chemical molecular structure of polyethylene terephthalate (PET), which is the surface chemical substance of DMD insulation paper.

TABLE 2. Basic parameters of DMD insulation paper at power frequency.

Volume Resistivity	Relative Permittivity	Loss Factor	Thermal Resistance	Breakdown Field
1.0×10^{14} (Ω · m)	3.0	0.008	*F* grade	22 (kV/mm)

composite paper with a thickness of 0.3 mm, which is widely used as inter-turn insulation in HV-HF transformers. DMD insulation paper is made of high-melting polyester film and polyester fiber non-woven fabric made by hot rolling. The main surface chemical substance of DMD insulation paper is the polyethylene terephthalate (PET), and its molecular chain structure is shown in Fig. 5. Meanwhile, the basic parameters of DMD paper at power frequency are listed in Table 2. Before the tests, a uniform boost method with a boost rate of 0.5 kV/s was used to determine the breakdown voltage U_s and the partial discharge inception voltage U_0. During the PD tests, the output voltage of the power source was limited to the range $[U_0, U_s]$ to prevent damage to spectrum analyzer due to the intense optical radiation caused by breakdown.

For air corona, the detection position of the fiber probes is the needle area. For partial discharge of gas-solid insulation, the detection position of the fiber probes is the junction area of the electrode, air, and solid dielectric, as shown in Fig. 6.

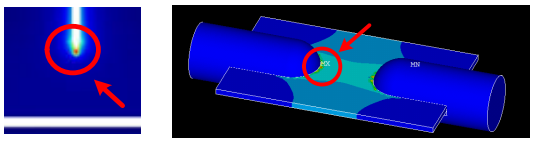

FIGURE 6. Schematic diagram of the fiber probe detection point. (a) Needle-plate electrode. (b) Finger electrode.

III. SPECTRUM ANALYSIS OF AIR CORONA

A. CHARACTERISTIC SPECTRUM OF AIR CORONA

Air is mainly composed of N_2, O_2, a small amount of CO_2, H_2O, and a variety of inert gases. When the high-frequency voltage was applied to the needle, particles existing in the non-uniform electric field region near the needle electrode absorbed energy and reached an excited state E_q. Once the particles transitioned from the excited state E_q to a lower energy state E_p, energy is released in the form of heat and light radiation, and the emission spectrum is generated. The energy provided by transition between specific energy levels, which determines the wavelength of the emission spectrum caused by partial discharges, as shown in equation (1). Therefore, the qualitative analysis can be performed on the type of particles that undergo an energy level transition based on the

wavelength of spectrum.

$$\lambda = \frac{c}{v} = \frac{hc}{E_q - E_p} \tag{1}$$

where λ is the wavelength of spectrum, c is the lightspeed, v is the photon frequency, h is the Planck constant, E_q is the energy of the excited state, E_p is the energy of the lower energy level or the ground state.

The spectral characteristics of air corona under high-frequency voltages were studied based on the needle-plate insulation model shown in Fig. 4(a). The spacing of the needle-plate electrode made of stainless steel was adjusted to 10 mm. The relative humidity of the air between the electrodes is (25±0.5) %, and the ambient temperature is (23±1) °C. Fig. 7 shows the emission spectrum of air corona in the wavelength range of 200 nm ∼1037 nm at a frequency of 5 kHz and a voltage amplitude of 7 kV. It can be seen from Fig. 7 that the emission spectrum of air corona under high-frequency has a series of characteristic peaks in the wavelength range of 315.64 nm ∼405.12 nm, which belongs to the near-ultraviolet region.

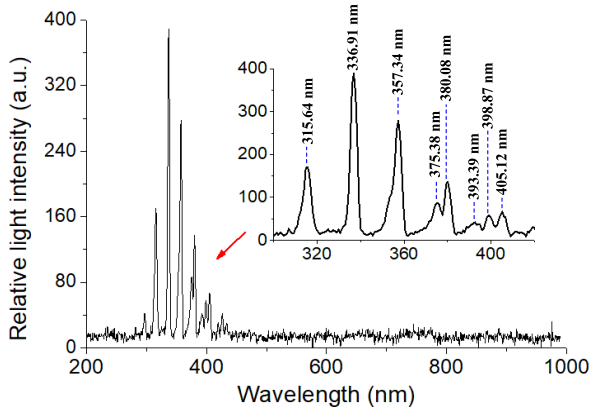

FIGURE 7. The characteristic emission spectrum of air corona at a frequency of 5 kHz and a voltage amplitude of 7 kV.

TABLE 3. Comparison between the measured and standard data.

Measured Spectral Data (nm)	Standard Spectral Data (nm)
315.64	315.93
336.91	337.13
357.34	357.69
375.38	375.54
380.08	380.49
393.39	394.30
398.87	399.84
405.12	405.94

Literature [20] gives the standard spectrum of the energy level transition of N_2 molecules. Table 3 is the comparison between the measured spectral wavelength and the standard spectral wavelength, which verifies that the characteristic spectrum of air corona under high-frequency square wave voltage is mainly caused by the energy level transition of N_2 molecules. The specific process of energy transition of N_2 molecules will be analyzed in detail below.

The characteristic spectral peaks of air corona discharge are produced by the process of excitation and transition of N_2 molecules. In the electric field, the N_2 molecules in the high field strength region absorb energy and transform from the ground state $N_2(X^1\Sigma_g^+)$ to the transition state $N_2(A^3\Sigma_u^+)$. With the continuous absorption of energy, the N_2 molecules with the transition state $N_2(A^3\Sigma_u^+)$ further transforms into the excited state $N_2(C^3\Pi_g)$, as shown in equations (2)-(3). However, the N_2 molecules with the excited state $N_2(C^3\Pi_g)$ will undergo a radiative transition due to their extremely unstable state, and rapidly transitions from the excited state $N_2(C^3\Pi_g)$ to the excited state $N_2(B^3\Pi_g)$ of a lower energy level. During the energy level transition, N_2 molecules will release energy in the form of light radiation to produce spectral characteristic peaks in a specific wavelength range, as shown in equation (4).

$$e_1 + N_2(X^1\Sigma_g^+) \rightarrow N_2(A^3\Sigma_u^+) \tag{2}$$

$$e_2 + N_2(A^3\Sigma_u^+) \rightarrow N_2(C^3\Pi_g) \tag{3}$$

$$N_2(C^3\Pi_g) = N_2(B^3\Pi_g) + hv \tag{4}$$

where $N_2(X^1\Sigma_g^+)$ is the ground state, $N_2(A^3\Sigma_u^+)$ is the transition state, $N_2(C^3\Pi_g)$ and the $N_2(B^3\Pi_g)$ are the excited states with different energy levels, e_1 and e_2 are the energy absorbed by the N_2 molecules in the high frequency electric field, $e_1 \geq 6.17$ eV and $e_2 \geq 4.9$ eV.

B. INFLUENCE FACTORS OF AIR CORONA SPECTRUM

In the preliminary experiment in the frequency range of 1 kHz∼20 kHz, the partial discharge inception voltage of the air corona is 6.5 kV∼7 kV, and the breakdown voltage is 10 kV∼10.5 kV. Therefore, the applied voltage in the spectral characteristics tests of the air corona should be lower than 10 kV to prevent damage to the spectrum analyzer due to the intense optical radiation caused by instant breakdown. Fig. 8 shows the variations of the emission spectrums with frequency at different voltages in the near-ultraviolet region where the emission spectrum caused by air corona appears. It can be seen from Fig. 8 that the wavelengths of spectrum peaks have not changed, indicating that the energy provided by the electric field with the frequency of 1∼20 kHz still makes N_2 molecules transition in the form of equation (2)-(4). Moreover, the maximum relative light intensity of air corona increases with the increase of the voltage amplitude at the same test frequency. When the voltage amplitude is increased from 7 kV to 9 kV, the maximum relative light intensity of the air corona increases to 1.75∼2.31 times the original value at a specific test frequency. The results will be explained from the perspective of spectrum formation.

The energy level transition of N_2 molecules in the high-field-strength region due to energy absorption occurs when a high-frequency voltage is applied to the needle electrode, which is the main cause of emission spectrum. The increase

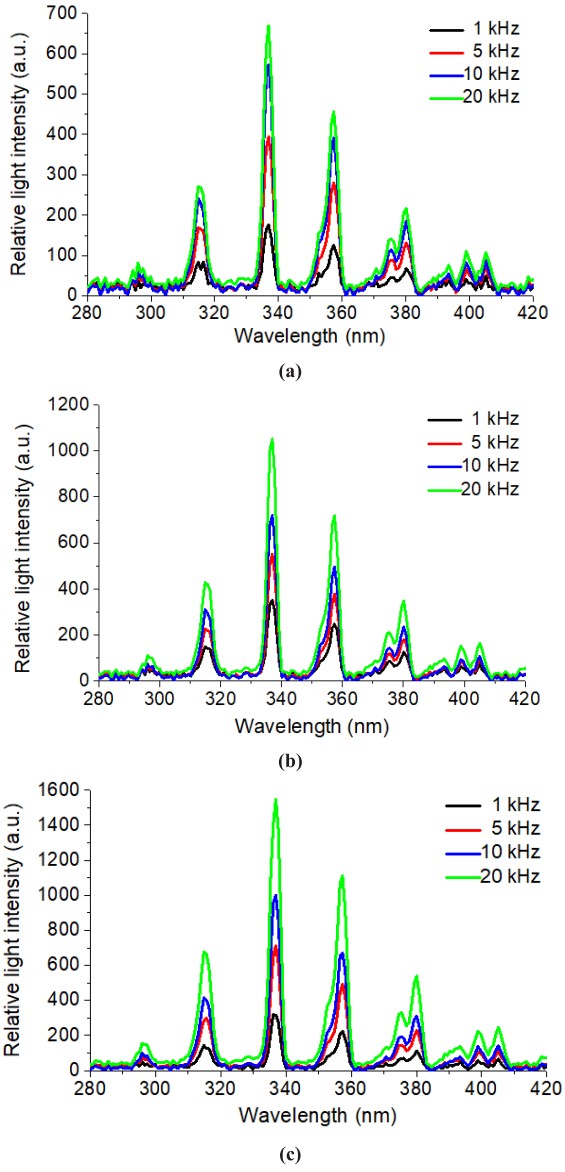

FIGURE 8. The variation of the emission spectrums with the frequency at different voltage amplitudes. (a) 7 kV. (b) 8 kV. (c) 9 kV.

of the voltage amplitude causes the electric field strength between the needle and plate electrode to increase, and the total optical radiation energy released when a larger number of N_2 molecules transition from the excited state $N_2(C^3\Pi_g)$ to the lower energy state $N_2(B^3\Pi_g)$ increases.

In addition to energy level transitions, the increase in voltage amplitude also promotes the increase of relative light intensity from the perspective of particle ionization and collision, as shown in Fig. 9. In the whole process of air corona, positive ions generated by ionization near the needle move toward the cathode under the electric field and collide with the cathode to generate high-energy free electrons. The free electrons will collide with N_2 molecules in the air, which promotes the generation of the excited state N_2 molecules, leading to an increase in the number of N_2 molecules involved in energy level transitions and an increase in the light intensity.

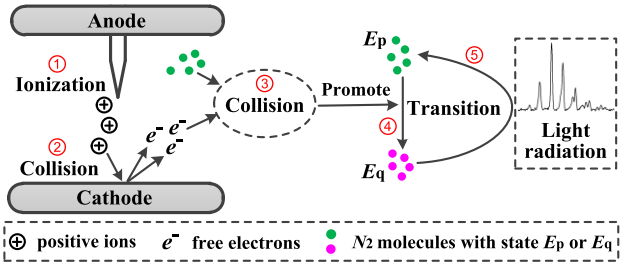

FIGURE 9. The impact of particle ionization and collision on the energy level transitions of N_2 molecules and light radiation during air corona.

In the process of air corona, the impact of particle collisions on the light intensity of the spectrum becomes more apparent as the voltage increases.

It can be seen from Fig. 8 that the relative light intensity in the wavelength range of 315.64∼405.12 nm gradually increases with the increase of test frequency. Under the same voltage amplitude, when the frequency is increased from 1 kHz to 20 kHz, the maximum relative light intensity increases to 3.01∼4.88 times of the original value. Some studies have shown that the increase in frequency will lead to a significant increase in the number of discharges per unit time, but the amount of partial discharge each time will decrease with the increase in frequency because the total energy in the total discharge cycle is constant [9], [21]. Based on the above test results, it can be inferred that the energy of each partial discharge injected into the electric field is still higher than 6.17 eV, which is the minimum energy value required for the energy level transition of N_2 molecules although the energy produced per air discharge decreased when the frequency is increased from 1 kHz to 20 kHz. The following will verify the rationality of the above analysis from the changes in the total number of photons and the ablation results of the needle electrodes.

In fact, the light intensity is equivalent to the number of photons received by the spectrum analyzer in a specific integration time, and the total number of photons in a certain wavelength band can be calculated by equation (5).

$$M = \int_{\lambda_1}^{\lambda_2} I(\lambda) d\lambda \tag{5}$$

where λ is the wavelength of spectrum, $I(\lambda)$ is the light intensity at wavelength λ, M is the total number of photons in the wavelength range from λ_1 to λ_2.

Fig. 10 shows the variation of the number of photons with frequency in the near-ultraviolet wavelength range where the spectrum of air corona is located. It can be seen from Fig. 10 that the number of photons increases with the increasing frequency at the same voltage amplitude. When the frequency is increased from 1 kHz to 20 kHz, the total number of photons increases to 3.38∼5.03 times the original value, which proves that the energy generated by each discharge still meets the needs of the energy transition of N_2.

Meanwhile, the increase in test frequency increases the number of corona discharges per unit time, leading to a

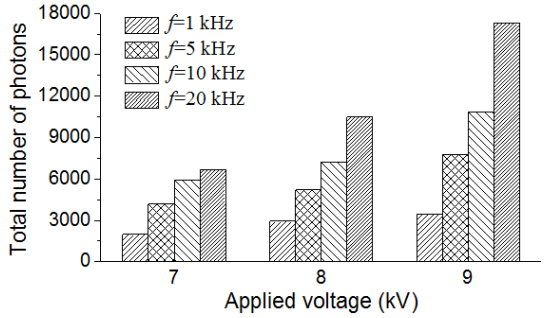

FIGURE 10. The variation of the total number of photons with frequency in the near-ultraviolet wavelength range (200~400 nm).

sharp increase in the number of charged particles produced by ionization and collisions in the electric field between the needle and the plate electrode. Once air breakdown occurs, the higher the test frequency, the more severe the ablation caused by larger number of charged particles, as shown in Fig. 11. The above analysis helps explain the test results that the spectral intensity increases with the test frequency.

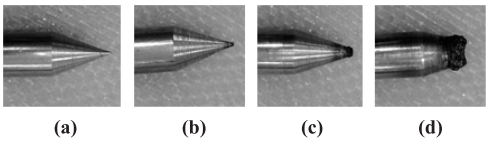

FIGURE 11. The ablation results of the needle after each breakdown at different frequencies. (a) 1 kHz. (b) 5 kHz. (c) 10 kHz. (d) 20 kHz.

IV. SPECTRUM PROPERTIES OF PARTIAL DISCHARGE ON GAS-SOLID SYSTEM

A. CHARACTERISTIC SPECTRUM ANALYSIS

The spectral characteristics of partial discharge in the gas-solid insulation system were studied based on the insulation model shown in Fig. 4(b). The pre-discharge test results of the gas-solid insulation system show that the partial discharge inception voltage is basically not affected by the test frequency, while the flashover voltage decreases significantly with the increase in frequency. When the voltage frequency is increased from 1 kHz to 20 kHz, the flashover voltage of the gas-solid insulation system drops about 3.5 kV, while the partial discharge inception voltage of the gas-solid insulation system is still remaining at 10.5 kV~11 kV, as shown in Fig. 12.

Fig. 13 is the characteristic spectrum of partial discharge on air-DMD paper insulation system, indicating that the partial discharges at the junction of the gas-solid system have band spectrums in the visible light region of 650 nm~780 nm and the near-infrared light region of 860 nm~900 nm except for the near-ultraviolet spectrum generated by the energy level transition of N_2 molecules. In fact, the emission spectrums in the visible and near-infrared light regions are caused by the energy level transitions of outer electronics and the vibrations of chemical bonds of the molecules in high-frequency high-voltage electric field.

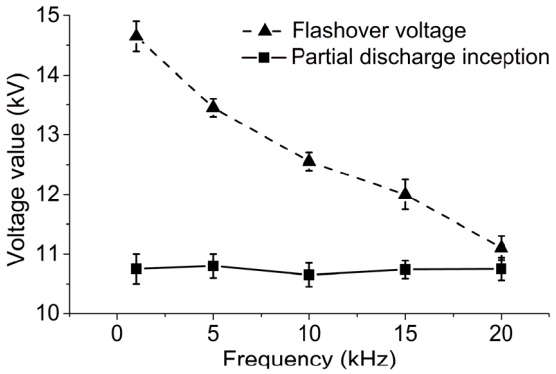

FIGURE 12. The variation of the partial discharge inception voltage and flashover voltage of gas-solid insulation system with voltage frequency.

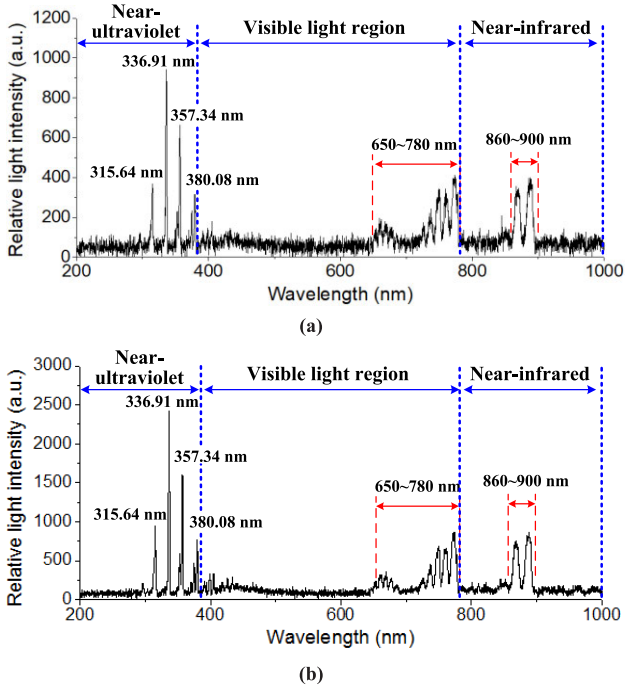

FIGURE 13. The characteristic emission spectrum of partial discharge on air-DMD insulation at a frequency of 5 kHz. (a) 11 kV. (b) 12 kV.

The main chemical substance that make up DMD paper is the PET, and the molecular chain structure of the PET has been shown in Fig. 5. The band-shaped spectrum in the visible light region of 650~780 nm is caused by the energy level transition of the outer electrons of the PET molecule, and the band-shaped spectrum in the near-infrared wavelength range of 860~900 nm is the result of energy transition due to the expansion or bending vibration of the C-H chemical bond on the PET molecule. Fig. 14 is the schematic diagram showing the stretching and bending vibrations of C-H chemical bonds of the PET molecules on the surface of the dielectric.

B. THE INFLUENCE OF FREQUENCY ON PARTIAL DISCHARGE OF GAS-SOLID INSULATION

In order to study the influence of frequency on the spectral properties of partial discharge, the test of gas-solid system was carried out at 12 kV and a frequency range of 1~20 kHz.

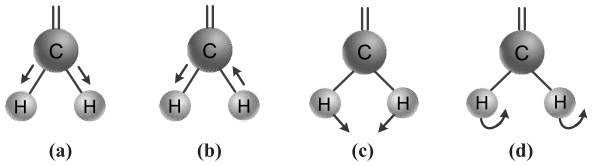

FIGURE 14. The stretching and bending vibrations of C-H chemical bonds of the PET molecules. (a) Symmetric stretch. (b) Asymmetric stretch. (c) In-plane bending. (d) Out-of-plane bending.

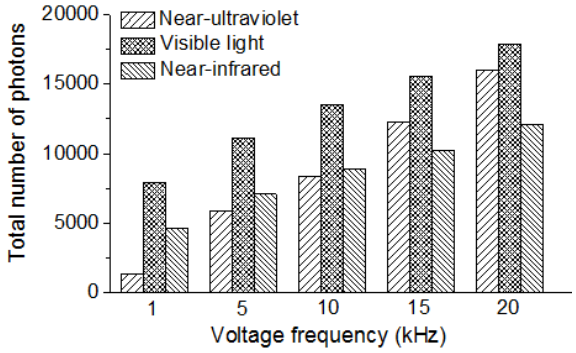

FIGURE 15. The variation of the number of photons in different bands produced by PDs of gas-solid insulation with test frequency at 11 kV.

Fig. 15 shows the variation of the number of photons in different bands produced by the partial discharge of gas-solid insulation with frequency. It can be seen from Fig. 15 that the total number of photons in the near-ultraviolet, near-infrared and visible range of the emission spectrum of partial discharge increases with the increasing frequency. Among them, the maximum raising rate appears in the near-ultraviolet, indicating that the influence of frequency on the energy level transition of N_2 molecules is much than the influence on the vibration of the C-H chemical bond and the energy transitions of outer electronics of molecules.

At present, most researchers believe that the secondary electron emission avalanche (SEEA) model can analyze the development stage of the surface discharge process [22]. The SEEA model considers that the discharge begins at the junction of electrode, gas and solid dielectric, where the local electric field is the highest. The field emission effect causes the initial electrons to bombard the surface of the dielectric, which continues to develop and forms the electron avalanche. Throughout the development of surface discharge, the contact surface between insulation paper and air forms a three-layer structure consisting of a micro-surface layer, a gas adsorption layer and a plasma layer. The electrons hit the micro-surface of the insulation material to release gas molecules, and the C-H bonds in the PET molecules can absorb gas and impurities in the air, so that a plasma layer is formed on the surface of the dielectric. The existence of the plasma layer promotes the uneven distribution of the surface charges and accelerates the development of surface discharge, as shown in Fig. 16.

The emission spectrum measured in this experiment are mainly generated in the initial and early development stages of surface discharges. For the initial stage of discharge, the increase in frequency increases the number of PDs per

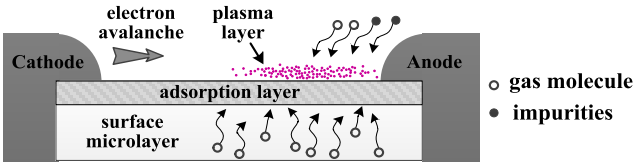

FIGURE 16. The effect of gas and impurities on the surface discharge.

unit time, and more N_2 molecules in the electric field within a unit time undergo energy level transitions, resulting in an increase in the light intensity in the near ultraviolet region as the frequency increases. Meanwhile, the increase in the frequency also causes the surface of dielectric to withstand greater polarization loss and fatigue shock, which promotes the energy level transition of the C-H chemical bonds and the outer layer electrons of the PET molecule, and finally leads to the increase in relative light intensities in the near-infrared light and visible light regions. After a long period of PDs, the influence of frequency on polarization loss and fatigue impact is visualized. Fig. 17 shows the microscopic conditions of DMD paper after 20 minutes of withstand voltage under the scanning electron microscope (SEM), indicating that the degree of insulation damage becomes more serious as the frequency increases, which to a certain extent verifies the correlation between the polarization loss and fatigue shock of the PET molecule and test frequency.

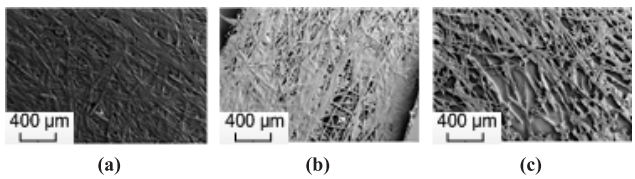

FIGURE 17. The surface conditions of the DMD paper after 20 minutes of withstand voltage under the SEM. (a) 1 kHz. (b) 5 kHz. (c) 10kHz.

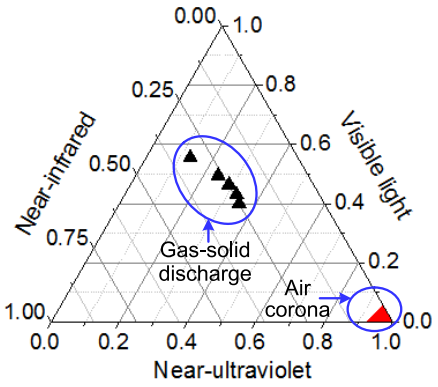

FIGURE 18. Comparison of the ratio of photons in different spectral regions between two types of partial discharges.

For the development stage of surface discharge, the increase in frequency leads to a decrease in the dissipation time of the charges on the surface of the dielectric, and the accumulation of charges accelerates the development of the electron avalanche. The plasma layer forms a stronger adsorption effect on gas molecules in the air, and then a

denser behavior of energy level transition of N_2 molecules occurs on the surface of the insulation dielectric, resulting in the maximum increase in the relative light intensity with increasing frequency in the near ultraviolet region.

According to the above analysis results, the characteristic spectrums produced by air corona and gas-solid insulation partial discharge are obvious different in the frequency range of 1 kHz∼20 kHz, which preliminarily shows that it is feasible to use the emission spectrum detection method to identify the type of discharge faults, as shown in Fig. 18. Therefore, optical diagnostic criteria for partial discharges for HV-HF transformers will be studied in future research.

V. CONCLUSION

In this paper, we have tested the emission spectrums of air corona and gas-solid insulation partial discharge under high frequency square wave voltage. The characteristic spectrum of air corona is composed of the near-ultraviolet spectrum in the wavelength range of 315.64∼405.12 nm, which is caused by the energy level transition of N_2 molecules. The spectral intensity of air corona is positively correlated with voltage amplitude and frequency, because the energy of each partial discharge injected into the electric field is still higher than the minimum energy value required for the energy level transition of N_2 molecules although the energy produced per air discharge decreased when the voltage frequency is increased from 1 kHz to 20 kHz.

In addition, the partial discharges of the gas-solid system have band spectrums in the visible light region of 650∼780 nm and the near-infrared light region of 860∼900 nm except for the near-ultraviolet spectrum generated by the energy level transition of N_2 molecules. The emission spectrums in the visible and near-infrared light regions are caused by the energy level transitions of outer layer electronics and the vibrations of C-H chemical bonds of the PET molecules in high-frequency high-voltage electric field. According to the SEEA model, the reason the number of photons in the near-infrared and visible range of the emission spectrum of gas-solid discharge increases with the increasing frequency is the increase in polarization loss and fatigue shock and the decrease in dissipation time of surface charges of dielectric.

The analysis results of this paper preliminarily verify the feasibility of applying the emission spectrum diagnostic method to partial discharge of air corona and surface discharge at the junction of gas-solid insulation system under high-frequency square wave voltages. However, in addition to the above two typical forms of partial discharges, there are also partial discharges inside the solid dielectrics. The applicability of emission spectrometry for detecting other different forms of PDs still needs further studies. In future research, we will improve the optical diagnostic criteria for PDs of different insulation fault types under high frequency square wave voltages, and try to establish the relationship between emission spectrum properties and more physical quantities such as space charge and dielectric surface charge to provide reliable theoretical basis for the optical on-line monitoring of partial discharge faults in high-voltage high-frequency transformer.

REFERENCES

[1] I. Syed and V. Khadkikar, "Replacing the grid interface transformer in wind energy conversion system with solid-state transformer," *IEEE Trans. Power Syst.*, vol. 32, no. 3, pp. 2152–2160, May 2017.

[2] M. Liserre, G. Buticchi, M. Andresen, G. De Carne, L. F. Costa, and Z.-X. Zou, "The smart transformer: Impact on the electric grid and technology challenges," *IEEE Ind. Electron. Mag.*, vol. 10, no. 2, pp. 46–58, Jun. 2016.

[3] S. Roy, A. De, and S. Bhattacharya, "Current source inverter based cascaded solid state transformer for AC to DC power conversion," in *Proc. Int. Power Electron. Conf.*, Hiroshima, Japan, May 2014, pp. 651–655.

[4] B. Chen and L. Li, "Semi-empirical model for precise analysis of copper losses in high-frequency transformers," *IEEE Access*, vol. 6, pp. 3655–3667, Jan. 2018.

[5] Y. Zhao, G. Zhang, R. Guo, and F. Yang, "The breakdown characteristics of thermostable insulation materials under high-frequency square waveform," *IEEE Trans. Dielectr. Electr. Insul.*, vol. 26, no. 4, pp. 1073–1080, Aug. 2019.

[6] M. Mogorovic and D. Dujic, "100 kW, 10 kHz medium-frequency transformer design optimization and experimental verification," *IEEE Trans. Power Electron.*, vol. 34, no. 2, pp. 1696–1708, Feb. 2019.

[7] J. Zhang, Y. Du, Z. Li, and P. Wang, "Design of a medium frequency, high voltage transformer for power electronic transformer," in *Proc. IEEE Conf. Expo Transp. Electrific. Asia–Pacific*, Beijing, China, Aug. 2014, pp. 1–5.

[8] E. Kuffel, S. Grzybowski, and R. B. Ugarte, "Flashover across polyethylene and tetrafluoroethylene surfaces in vacuum under direct, alternating and surge voltages of various waveshapes," *J. Phys. D, Appl. Phys.*, vol. 5, no. 3, pp. 575–579, Mar. 1972.

[9] P. Wang, H. Xu, J. Wang, W. Wang, and A. Cavallini, "Effect of repetitive impulsive voltage duty cycle on partial discharge features and insulation endurance of enameled wires for inverter-fed low voltage machines," *IEEE Trans. Dielectr. Electr. Insul.*, vol. 24, no. 4, pp. 2123–2131, Sep. 2017.

[10] S. N. Rao and K. Elanseralathan, "Influence of switching frequency of the voltage waveforms on breakdown in twisted pairs," in *Proc. Int. Conf. Electr. Power Energy Syst.*, Bhopal, India, 2016, pp. 545–548.

[11] D. Wang, J. Tian, C. Mao, J. Lu, Y. Duan, J. Qiu, and H. Cai, "A 10-kV/400-V 500-kVA electronic power transformer," *IEEE Trans. Ind. Electron.*, vol. 63, no. 11, pp. 6653–6663, Nov. 2016.

[12] T. Czech, A. T. Sobczyk, and A. Jaworek, "Optical emission spectroscopy of point-plane corona and back-corona discharges in air," *Eur. Phys. J. D*, vol. 65, no. 3, pp. 459–474, Nov. 2011.

[13] S. A. Shcherbanev, I. U. Nadinov, P. Auvray, S. M. Starikovskaia, S. Pancheshnyi, and L. G. Herrmann, "Emission spectroscopy of partial discharges in air-filled voids in unfilled epoxy," *IEEE Trans. Plasma Sci.*, vol. 44, no. 7, pp. 1219–1227, Jul. 2016.

[14] J. Cen, P. Yuan, S. Xue, and X. Wang, "Spectral characteristics of lightning dart leader propagating in long path," *Atmos. Res.*, vols. 164–165, pp. 95–98, Oct. 2015.

[15] M. Koziol and Ł. Nagi, "Analysis of optical radiation spectra emitted by electrical discharges, generated by different configuration types of high voltage electrodes," in *Proc. IEEE 2nd Int. Conf. Dielectrics (ICD)*, Budapest, Hungary, Jul. 2018, pp. 1–4.

[16] K. Fujii, M. Yamada, A. Tanaka, and K. Kurosawa, "Emission spectrum of partial discharge light in SF_6 gas," in *Proc. Conf. Rec. IEEE Int. Symp. Electr. Insul.*, Baltimore, MD, USA, Jun. 1992, pp. 332–335.

[17] W. Zhao, X. Zhang, J. Jiang, and N. Wei, "Spectrum analysis of tip-plane corona discharges," (in Chinese), *Spectrosc. Spectral Anal.*, vol. 23, no. 5, pp. 955–957, Oct. 2003.

[18] M. Ren, B. Song, T. Zhuang, and S. Yang, "Optical partial discharge diagnostic in SF6 gas insulated system via multi-spectral detection," *ISA Trans.*, vol. 75, pp. 247–257, Apr. 2018.

[19] Y. Yan, N. Wang, C. Li, and H. Shu, "Experimental study of N2 in high voltage pulse corona discharge in air," (in Chinese), *Instrum. Anal. Monitor.*, vol. 1, no. 1, pp. 40–42, 2004.

[20] R. W. B. Pearse and A. G. Gaydon, *The Identification of Molecular Spectra*, 3rd ed. London, U.K.: Chapman & Hall, 1963. [Online]. Available: https://www.sciencedirect.com/science/article/abs/pii/0010218064900422

[21] T. Liu, Y. Xiao, Y. Lu, X. Huang, Q. Li, and Z. Wang, "Effect of voltage frequency on surface discharge characteristics and aging process," in *Proc. IEEE Electr. Insul. Conf.*, Baltimore, MD, USA, Jun. 2017, pp. 463–466.
[22] R. A. Anderson and J. P. Brainard, "Mechanism of pulsed surface flashover involving electron-stimulated desorption," *J. Phys. D, Appl. Phys.*, vol. 51, no. 3, pp. 1414–1421, Apr. 1980.

YIKUN ZHAO received the B.E. degree from China Agriculture University, Beijing, China, in 2016. He is currently pursuing the master's degree with the University of Chinese Academy of Sciences (UCAS). His research interests include the discharge properties of insulation materials and heat dissipation technology for high-voltage high-capacity high-frequency transformers.

YANFEI LI received the B.E. degree from Northeast Electric Power University, Jilin, China, in 2018. He is currently pursuing the master's degree with the University of Chinese Academy of Sciences (UCAS). His research interests include the fault diagnosis and online monitoring of power equipment and emission spectrum detection methods of partial discharge.

KANG LI (Member, IEEE) received the bachelor's degree from the Department of Electrical Engineering, Tsinghua University, in 2007, and the Ph.D. degree from the School of Information Science, Electrical, and Electronics Engineering, University of Chinese Academy of Sciences, in 2012. He is currently an Associate Professor with the Institute of Electrical Engineering, Chinese Academy of Sciences. His research interests include new type sensors and monitoring instruments of electric power transmission and transformation equipment.

DONG HAN received the B.S. degree in electrical engineering from Shandong University, Jinan, China, in 1997, and the M.S. and Ph.D. degrees from North China Electric Power University, Beijing, China, in 2005 and 2009, respectively. She is currently an Associate Professor with the Institute of Electrical Engineering, Chinese Academy of Sciences. Her research interests include electric equipment fault diagnosis and monitoring, multi-parameter uncertainty analysis, and emission spectrum detection method of partial discharge.

ZONGJIA QIU received the bachelor's degree from Beihang University, and the M.S. and Ph.D. degrees from the Beijing Institute of Technology. He is currently an Associate Researcher with the Institute of Electrical Engineering, Chinese Academy of Sciences. His research interests include the multi-parameter uncertainty analysis and emission spectrum detection method of partial discharge, the optical method of fault detection, and the status detection of electrical equipment.

GUOQIANG ZHANG received the B.E. degree from the Hebei University of Technology, Tianjin, China, in 1984, the M.E. degree from Tsinghua University, Beijing, China, in 1989, and the Ph.D. degree from North China Electric Power University. He worked in Tsinghua as a postdoctoral researcher from 2001 to 2003. After that, he worked as a Postdoctoral Researcher with the University of Cambridge from 2004 to 2005. Since 2005, he has been a Researcher with the Institute of Electrical Engineering, Chinese Academy of Sciences, Beijing. His research interests include high voltage insulation, new electrical equipment, intelligent power transmission, and transformation equipment.